Mechanics of Materials 12 (1991) 85–94
Elsevier



# The flow stress of dual-phase, non-hardening solids

G. Bao
*Materials Department, University of California, Santa Barbara, CA 93106, USA*

J.W. Hutchinson
*Division of Applied Sciences, Harvard University, Cambridge, MA 02138, USA*

and

R.M. McMeeking
*Departments of Materials and Mechanical Engineering, University of California, Santa Barbara, CA 93106, USA*

Received 1 October 1990

A dual-phase composite comprised of an isotropic distribution of two elastic–perfectly plastic phases is considered. Each phase is characterized by a Mises yield surface and its associated tensile flow stress. The limiting tensile flow stress of the composite is computed in terms of the flow stresses of the phases and their respective volume fractions using a fully non-linear self-consistent model which identifies one phase as particulate and the other as matrix. It is found that the uniform strain-rate upper bound, which is just the rule of mixtures in terms of the phase flow stresses, provides an excellent approximation to the composite flow stress as long as the flow stresses of the phases do not differ by more than a factor of two. The results are applied to obtain some insight into the effect of a non-uniform isotropic distribution of rigid particles in reinforcing an elastic–perfectly plastic matrix. By identifying the tensile flow stresses of the two phases with flow stresses of particle-rich and particle-poor regions, one can predict the dependence of the limit flow stress of the composite on certain types of non-uniform distributions of the rigid particle reinforcements.

## 1. Specification of the model

The composite solid to be analyzed is depicted in Fig. 1. It is comprised of an isotropic distribution of two perfectly bonded elastic–perfectly plastic phases. Each phase is characterized by a Mises yield surface:

$$\left(\tfrac{3}{2}s_{ij}s_{ij}\right)^{1/2} = \sigma_0^{(i)}, \quad i = 1, 2, \tag{1.1}$$

where $s_{ij}$ is the stress deviator. Attention is limited to the limit tensile flow stress $\bar{\sigma}_0$ of the composite. Under uniaxial stressing the elastic response of the composite and the transition to the limit stress depend on the elastic moduli of the phases, but $\bar{\sigma}_0$ does not. Thus $\bar{\sigma}_0$ depends on $\sigma_0^{(1)}$ and $\sigma_0^{(2)}$, on the volume fractions of the phases, $f^{(1)}$ and $f^{(2)} = 1 - f^{(1)}$, and on details of how the phases are distributed. It is this dependence which is addressed in this paper.

The uniform strain-rate upper bound to $\bar{\sigma}_0$ is readily found to be

$$\bar{\sigma}_0 = f^{(1)}\sigma_0^{(1)} + f^{(2)}\sigma_0^{(2)}, \tag{1.2}$$

which is just the rule of mixtures for the flow stresses. Two types of approximations are made in obtaining an improved estimate of $\bar{\sigma}_0$. Firstly, any possible dependence of the limit yield surface of the composite on the third stress invariant, $\bar{s}_{ij}\bar{s}_{jk}\bar{s}_{ki}$, is neglected, and thus

$$\left(\tfrac{3}{2}\bar{s}_{ij}\bar{s}_{ij}\right)^{3/2} = \bar{\sigma}_0 \tag{1.3}$$

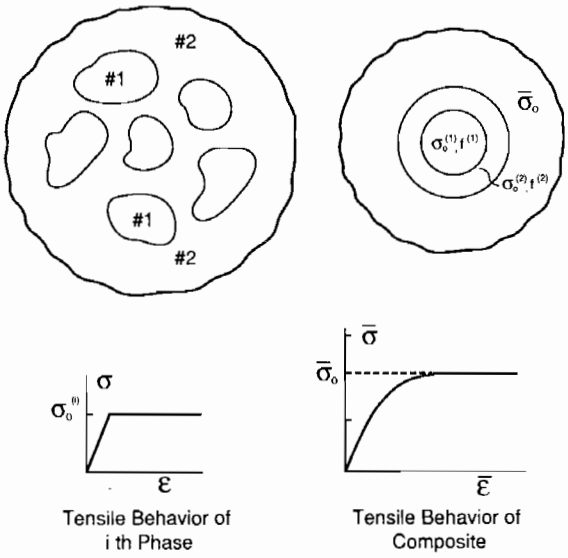


Fig. 1. Geometry of composite and self-consistent model. Tensile stress–strain behavior of the phases and the composite.

is taken to describe the composite limit yield surface. Secondly, a self-consistent scheme is used to model the distribution of the two phases and to thereby determine $\bar{\sigma}_0$.

The geometry of the self-consistent model is shown in Fig. 1. Versions of this same model have been used recently by Christensen (1990) for elastic systems and by Taggart and Bassani (1991) for particle-reinforced elastic–plastic solids. Weng (1990) has employed another self-consistent scheme to study the stress–strain behavior of dual-phase solids. His work will be discussed later. In the present model phase No. 1 is regarded as the "particulate phase" and occupies the spherical inclusion in the model with volume $f^{(1)}$. Phase No. 2, which is considered to be the "matrix phase", occupies the concentric spherical shell with volume $f^{(2)}$. The two phases are embedded in an infinite solid whose limit yield surface is that of the composite (1.3). As already noted, the limit yield stress of the actual composite (or as predicted by the self-consistent model) does not depend on the elastic moduli of the phases. The self-consistent prediction of $\bar{\sigma}_0$ is also independent of the elastic moduli assigned to the infinite outer region and to its transition stress–strain behavior. Thus, without any approximation to the self-consistent computation of $\bar{\sigma}_0$, one can take the elastic moduli of the two phases and that of the outer region to be identical. Moreover, for computational purposes, one can take the outer region to be elastic–perfectly plastic. That is, one need not correctly model the transition stress–strain behavior of the composite within the outer region in order to compute $\bar{\sigma}_0$. These two steps were taken in performing the computations carried out below.

The self-consistent model is fully nonlinear in the sense that each of the two phases is taken to be non-hardening and to obey flow theory plasticity, as is also the case for the infinite outer region. A finite element method is used to solve for the stresses and strain-rates in the limit state, as will be described later. To compute $\bar{\sigma}_0$, a strain rate with non-zero components,

$$\dot{E}_{33} = \dot{E}, \quad \dot{E}_{11} = \dot{E}_{22} = -\tfrac{1}{2}\dot{E}, \tag{1.4}$$

is imposed remotely on the outer region. The remote strain $E$ is incremented until a limiting stress distribution is attained. Since the self-consistent model is isotropic, the choice of the axes of principal straining is immaterial.

Two different self-consistent equations for determining $\bar{\sigma}_0$ were considered. For *stress averaging* we require that in the limit state

$$\bar{\sigma}_0 \dot{E} = \int_V \sigma_{ij} \dot{E}_{ij} \, \mathrm{d}V, \tag{1.5}$$

where the volume average is carried out over the unit volume comprising phases No. 1 and No. 2. This condition is equivalent to $\frac{2}{3}\bar{\sigma}_0 = \int_V s_{33} \, \mathrm{d}V$. For *strain-rate averaging* we require that the strain-rates in the limit state satisfy

$$\dot{E} = \int_V \dot{\epsilon}_{33} \, \mathrm{d}V. \tag{1.6}$$

These conditions are implicit equations which require iteration on $\bar{\sigma}_0$ in the computational process.

## 2. Numerical implementation

At any iterative step, a value is assigned to $\bar{\sigma}_0$, the limit state is computed, and one or the other of the self-consistent conditions (1.5) or (1.6), is

evaluated. Then a new estimate of $\bar{\sigma}_0$ is assigned using standard zero-crossing methods and the process is repeated until an accurate solution for $\bar{\sigma}_0$ is obtained.

The model geometry of Fig. 1 was truncated to a finite region with an outer spherical surface where the total volume of the three regions was 20 times the volume of the two inner regions containing the two phases. Uniform straining displacement rates, $\dot{U}_i$, were imposed on the outer surface where $\dot{U}_i = \dot{E}_{ij} x_j$.

For a given value of $\bar{\sigma}_0$, the computational problem for the limit state is axisymmetric. The ABAQUS computer code employing 8-noded quadrilateral elements was used to carry out the calculations. Numerical experiment together with mesh refinement was used to arrive at the meshes used. Typically, a total of 432 elements were used with 216 of these employed in the outer region. As described in the previous section, the stress and strain-rate distribution in the limit state were obtained by incrementing $E$. The process was started from a uniform state of zero stress, although this is not essential. One advantage of the computational procedure is that errors incurred during the approach to the limit state are "washed out" as $E$ increases. It was convenient to replace (1.5) and (1.6) by their respective equivalents:

$$\bar{\sigma}_0 \dot{E} = \int_S \sigma_{ij} n_j \dot{U}_i \, dS \tag{2.1}$$

and

$$\dot{E} = \int_S \dot{u}_3 n_3 \, dS, \tag{2.2}$$

where the integration is over the surface of the sphere containing phases No. 1 and No. 2 and $\boldsymbol{n}$ is the outward unit normal to this surface.

Values for $\bar{\sigma}_0$ were calculated for $\sigma_0^{(1)}/\sigma_0^{(2)} = 0.2$, 0.5, 2, 5 and 20 at each of the following values of $f^{(1)}$: 0.1, 0.2, 0.3, 0.4, 0.5, 0.6, 0.7, 0.8, 0.9 and 0.95. Of course, $\bar{\sigma}_0 = \bar{\sigma}_0^{(1)}$ for all $f^{(1)}$ when $\sigma_0^{(1)}/\sigma_0^{(2)} = 1$.

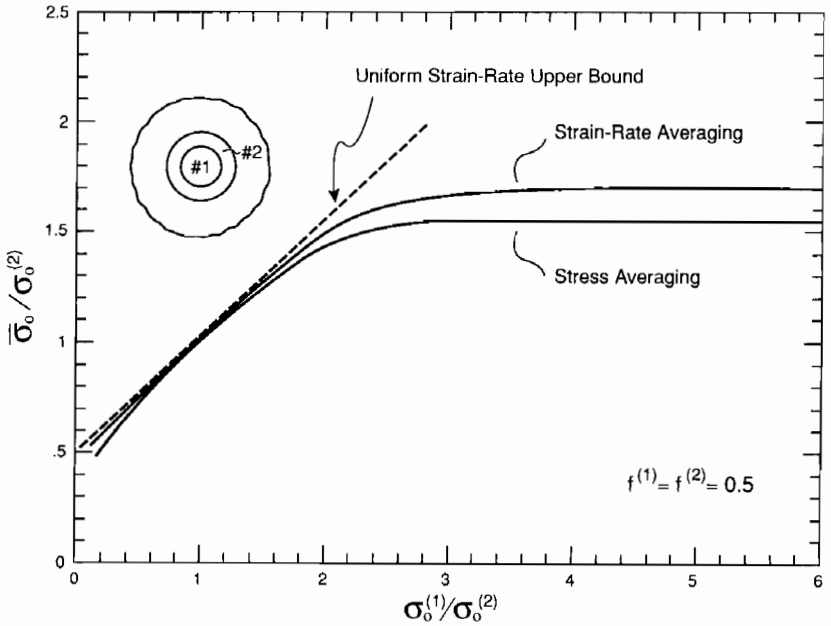


Fig. 2. Normalized limit flow stress of composite as a function of the ratio of the phase flow stresses for $f^{(1)} = f^{(2)} = \frac{1}{2}$. Phase No. 1 is the particle phase and No. 2 is the matrix phase.

## 3. Predictions

To begin, take the volume fractions of the phases to be equal, i.e. $f^{(1)} = f^{(2)} = 0.5$. Figure 2 displays the dependence of $\bar{\sigma}_0/\sigma_0^{(2)}$ on the flow stress ratio of the phases as determined from the two self-consistent equations. There is some difference in the predictions depending on which self-consistent condition is used. When the particulate phase (No. 1) is very hard compared to the matrix phase, $\bar{\sigma}_0$ as predicted from the strain-rate averaging condition is about 10% higher than the stress averaging prediction. For each condition, the particle phase is predicted to be effectively rigid when its flow stress is about 2.5 times the matrix flow stress. The composite flow stress is then a little more than 1.5 matrix flow stress. The other limit, when the particle phase is very soft compared to the matrix, corresponds to a matrix containing regions which are free to distort but which are not free to dilate. This limit is not the same as that for a matrix containing voids with traction-free surfaces.

The uniform strain rate upper bound to $\bar{\sigma}_0$ from (1.2) is also shown in Fig. 2, i.e. for $f^{(1)} = f^{(2)} = \frac{1}{2}$,

$$\bar{\sigma}_0/\sigma_0^{(2)} = \tfrac{1}{2}\left(1 + \sigma_0^{(1)}/\sigma_0^{(2)}\right). \tag{3.1}$$

The bound is a good approximation to $\bar{\sigma}_0$ for a phase flow stress ratio satisfying

$$\tfrac{1}{2} \leqslant \sigma_0^{(1)}/\sigma_0^{(2)} \leqslant 2. \tag{3.2}$$

There exists other examples which corroborate the ability of the uniform strain-rate upper bound to provide a good approximation to more elaborate models for predicting the limit flow stress of elastic–perfectly plastic systems as long as the heterogeneity of the local flow stresses is not too large. For example, it has recently been shown (Dendievel, Bonnet and Willis, 1990) that the uniform strain rate bound for a polycrystal comprised of randomly orientated fcc single crystals is only slightly higher than a new, tighter upper bound. The result was obtained for pure power law behavior and the conclusion applies for all values of the stress exponent from about 2 to $\infty$ (perfect plas-

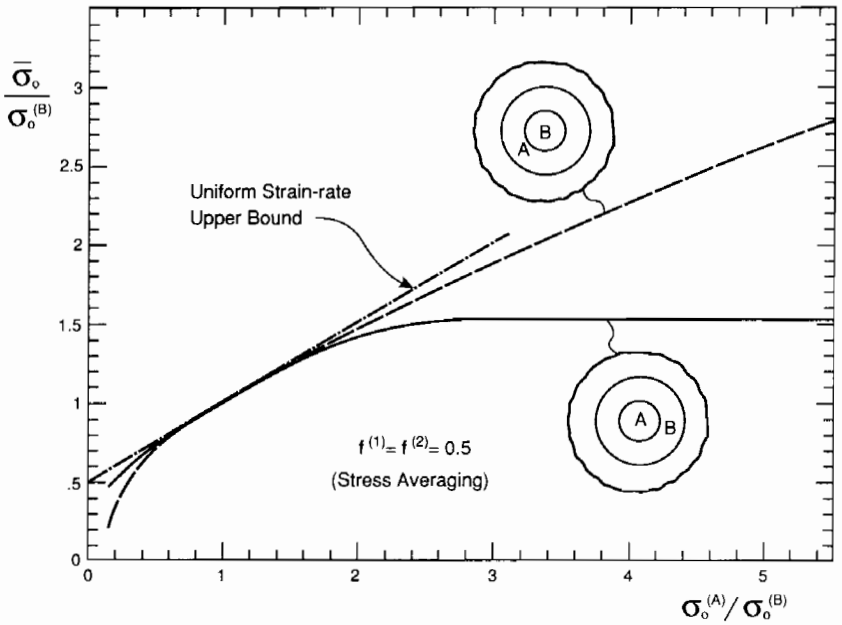


Fig. 3. Effect of interchanging the roles of the particle and matrix phases for the case of equal volume fractions of the two phases.

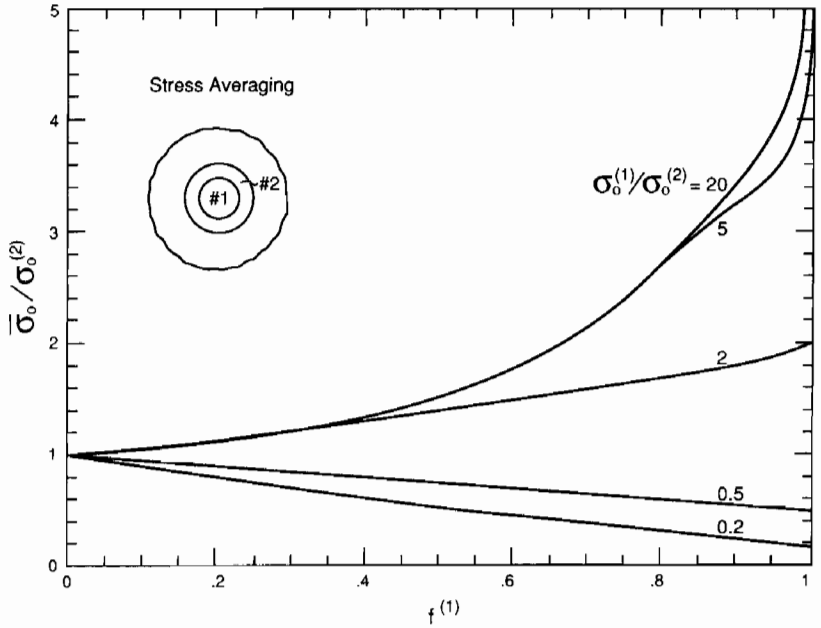


Fig. 4. Normalized limit flow stress of the composite versus volume fraction of the particle phase based on the stress averaging self-consistent equation.

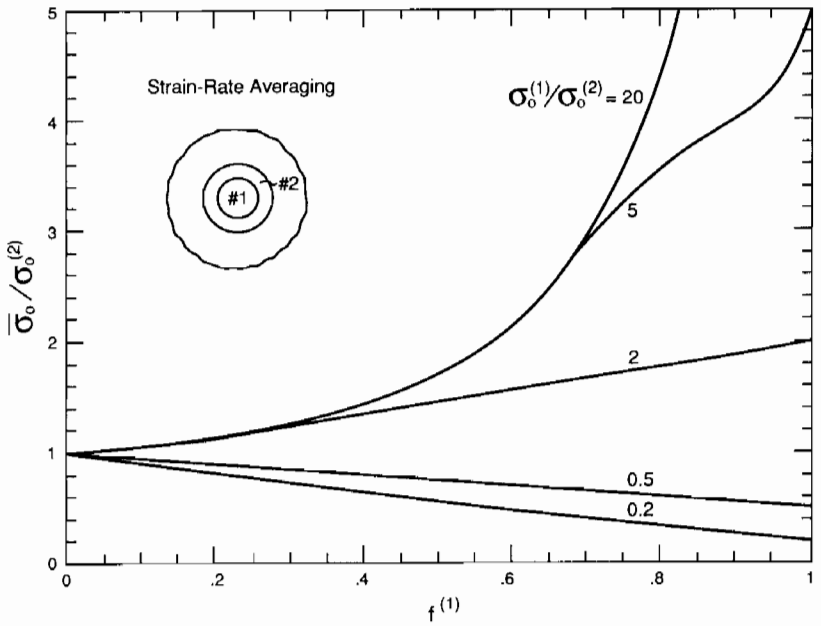


Fig. 5. Normalized limit flow stress of the composite versus volume fraction of the particle phase based on the strain-rate averaging self-consistent equation.

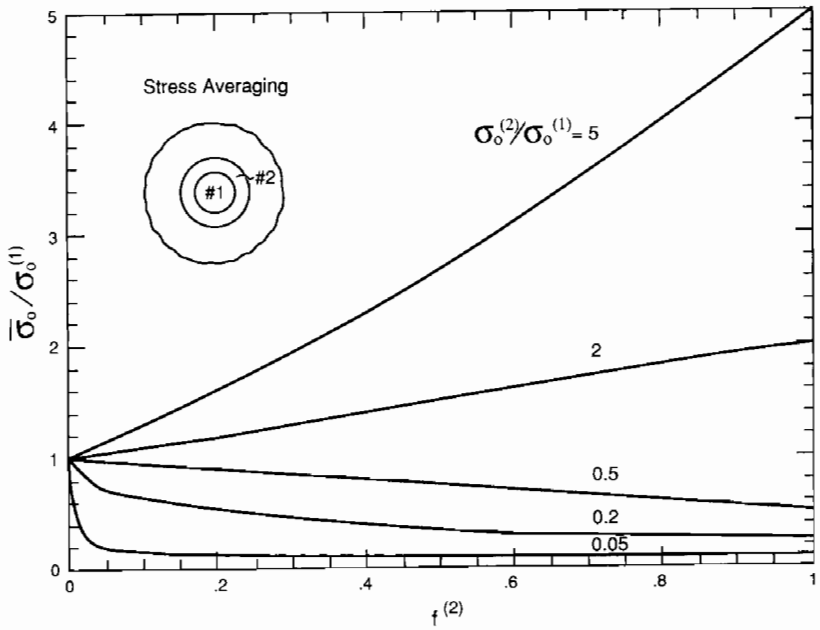


Fig. 6. Normalized limit flow stress of the composite versus volume fraction of the matrix phase based on the stress averaging self-consistent equation.

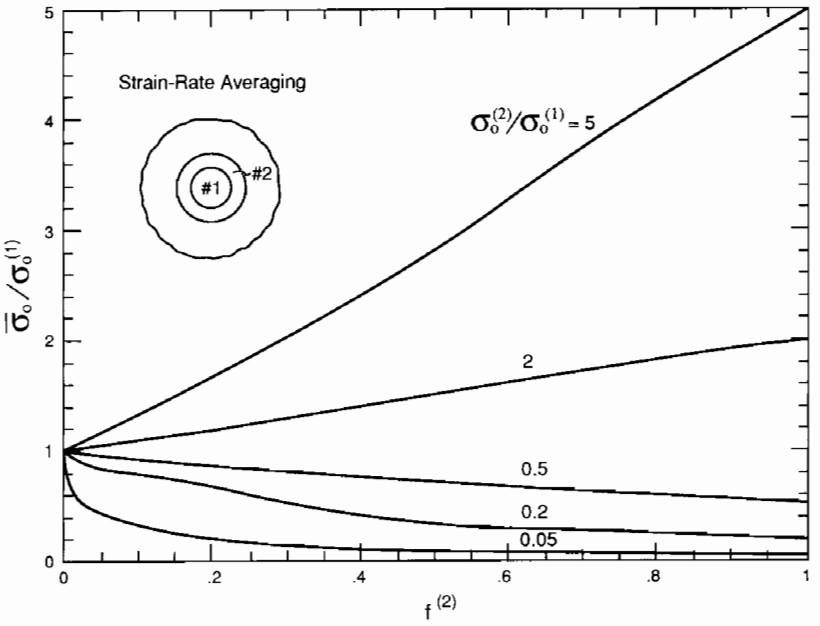


Fig. 7. Normalized limit flow stress of the composite versus volume fraction of the matrix phase based on the strain-rate averaging self-consistent equation.

ticity). Similar favorable performance of the uniform strain rate upper bound has been found by Hutchinson (1976, 1977) based on comparisons with self-consistent calculations for polycrystals comprised of single crystals whose slip systems have differing hardnesses, as long as the relative differences are not larger than about a factor of two.

The results of Fig. 2 are replotted in Fig. 3 in a way which reveals the differing roles of the particle and matrix phases. Here, to avoid confusion with prior notation, the two materials are denoted by A and B. The solid curve, which is taken directly from Fig. 2, has A as the particle phase, while the dashed curve gives the prediction when B is the particle phase. For both curves, $\bar{\sigma}_0$ is normalized by the flow stress of material B. Within the range,

$$\tfrac{1}{2} < \sigma_0^{(A)}/\sigma_0^{(B)} < 2, \tag{3.3}$$

there is relative little difference between the two predictions. This suggests that the flow stress of a composite with equal volume fractions of isotropically distributed phases may not depend very strongly on other details of the geometry of the phases within the above range of flow stress ratios. Moreover, the upper bound (1.2) provides a good approximation to $\bar{\sigma}_0$ within this range.

The complete set of numerical results from the stress averaging condition are plotted in Fig. 4 and those from the strain-rate averaging condition are plotted in Fig. 5. In these two figures $\bar{\sigma}_0/\sigma_0^{(2)}$ is shown as a function of $f^{(1)}$ for various $\sigma_0^{(1)}/\sigma_0^{(2)}$. For completeness, the same data is replotted in Figs. 6 and 7 as $\bar{\sigma}_0/\sigma_0^{(1)}$ versus $f^{(2)}$ for various flow stress ratios. The following observations are based on the results in these figures.

Noting that the uniform strain rate upper bound to $\bar{\sigma}_0$ 91.2) is a linear function of $f^{(1)}$ (or $f^{(2)}$) with end values of $\sigma_0^{(1)}$ and $\sigma_0^{(2)}$, one sees that this bound provides a good approximation to the self-consistent predictions for phase hardness ratios satisfying $\sigma_0^{(1)}/\sigma_0^{(2)} \leqslant 2$. In words, the bound (1.2), which is simply the rule of mixtures, is a reasonably accurate estimate of $\bar{\sigma}_0$ as long as the flow stress of the particle phase is not more than about two times the flow stress of the matrix phase. Thus, the conclusion drawn from the results in Fig. 3 for $f^{(1)} = f^{(2)} = 0.5$ holds for all volume fractions of the phases. It appears that the geometry of the phases has relatively little effect on $\bar{\sigma}_0$ when there is less than a factor of 2 difference in the flow stresses of the phases.

The simple bound (1.2) overestimates $\bar{\sigma}_0$ when the particle phase hardness exceeds the matrix phase hardness by more than a factor of 2. The only significant differences between the stress-averaging and strain-rate averaging predictions show up in this range. In Figs. 4 and 5, the composite with $\sigma_0^{(1)}/\sigma_0^{(2)} = 20$ is, for all practical purposes a matrix containing rigid spherical particles. It has already been noted that the particle phase is effectively rigid for $\sigma_0^{(1)}/\sigma_0^{(2)} \geqslant 2.5$ when $f^{(1)} = 0.5$. When $\sigma_0^{(1)}/\sigma_0^{(2)} = 5$, the particle phase is effectively rigid for volume fractions as large as $f^{(1)} = 0.7$, or possibly 0.8, according to the self-consistent model.

Weng (1990) has carried out a study of the tensile stress–strain behavior of dual phase hardening metals using both a uniform strain rate procedure (the Taylor method) and an approximate version of Hill's (1965) incremental self-consistent model. While it is not possible to make direct comparisons between his predictions and those for the non-hardening solids considered here, there is a close parallel in some of the findings. As in the present study, Weng finds that the uniform strain rate procedure gives accurate predictions when the flow stress of the particle phase is less than that of the matrix phase while it overestimates the composite flow stress when the particle phase is significantly harder than the matrix phase. The effect of interchanging the particle and matrix phases predicted by the self-consistent model used by Weng is similar to that found in the present study.

## 4. Application to an elastic–perfectly plastic matrix reinforced by a non-uniform, isotropic distribution of rigid particles

The results of the previous section are now used to gain some insight into the role of non-uniformity in the distribution of rigid reinforcing

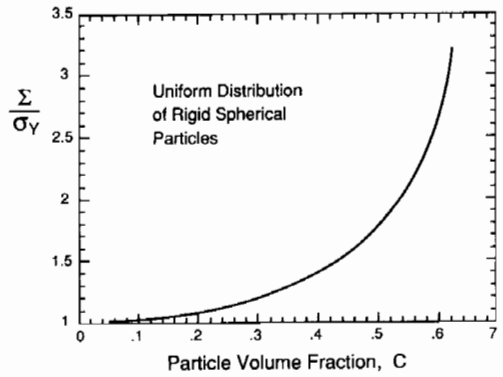


Fig. 8. Ratio of limit flow stress to matrix flow stress for a uniform distribution of equi-sized, rigid spherical particles with volume fraction $c$ embedded in an elastic–perfectly plastic matrix. The curve is based on the cell model calculation by Bao et al. (1991).

particles in strengthening an elastic-perfectly plastic matrix. The limit tensile flow stress $\Sigma$ is shown in Fig. 8 for an elastic–perfectly plastic matrix with tensile flow stress $\sigma_Y$ which is reinforced by a *uniform*, isotropic distribution of perfectly bonded, equi-sized, rigid spherical particles with volume fraction $c$. This result, $\Sigma(c)$, for the uniform distribution was computed by Bao et al. (1991) using a cell with approximate periodic-type boundary conditions to model the interaction between particles.

Now consider a *non-uniform*, isotropic distribution of equi-sized particles where, as depicted in Fig. 9, the matrix has sub-regions which are either particle-rich or particle-poor. To apply the results of the previous section, assume that the characteristic size of the sub-regions is large compared to the average spacing of the particles. Further, assume that the particles within each sub-region are distributed uniformly with volume fraction $c_1$ in sub-regions 1 and $c_2$ in sub-regions 2. For definiteness in applying the results of the previous section, suppose sub-regions 1 comprise the "particulate phase" with volume fraction $f^{(1)}$, and let sub-regions 2 be the "matrix phase" with volume fraction $f^{(2)}$, as in Fig. 9. The average volume fraction of the rigid particles, taken over both "phases", is

$$\bar{c} = f^{(1)}c_1 + f^{(2)}c_2, \tag{4.1}$$

where $f^{(1)} + f^{(2)} = 1$. The flow stresses of the sub-regions are identified according to (cf. Fig. 9)

$$\sigma_0^{(1)} = \Sigma(c_1) \quad \text{and} \quad \sigma_0^{(2)} = \Sigma(c_2). \tag{4.2}$$

Now the results of Section 3 can be applied to predict the dependence of the composite limit flow stress $\bar{\sigma}_0$ on the non-uniformity as measured, for example, by $c_1 - \bar{c}$. With $f^{(1)}$ (and therefore $f^{(2)}$) taken to prescribed, (4.1) requires

$$c_2 - \bar{c} = -\left(f^{(1)}/f^{(2)}\right)(c_1 - \bar{c}). \tag{4.3}$$

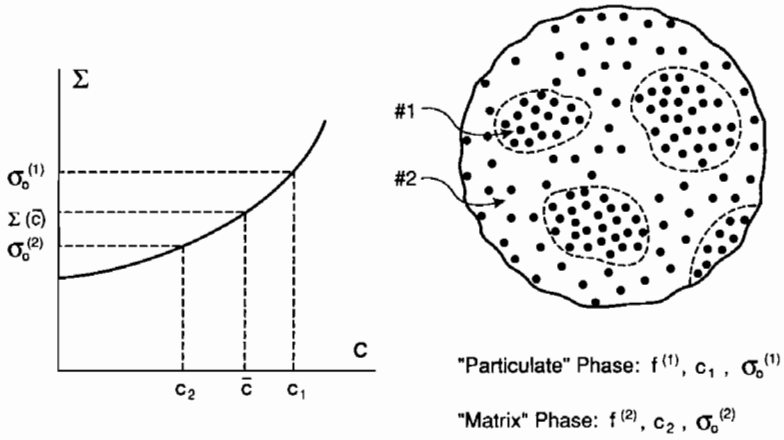


Fig. 9. Scheme for applying the results for the dual-phase composite to a matrix reinforced by equi-sized rigid particles which are non-uniformly distributed.

A specific example will be displayed below, but first a general result will be derived which applies when the non-uniformity is not too large.

Suppose that $c_1 - \bar{c}$ is such that the "phase" flow stresses in (4.2) differ by less than a factor of two. Then, as emphasized earlier, the simple rule of mixtures formula (1.2) can be used to predict $\bar{\sigma}_0$. For sufficiently small $c_i - \bar{c}$, truncated expansions of (4.2) can be used, i.e.

$$\sigma_0^{(i)} = \Sigma(\bar{c}) + \frac{\partial \Sigma(\bar{c})}{\partial c}(c_i - \bar{c}) + \frac{1}{2}\frac{\partial^2 \Sigma(\bar{c})}{\partial c^2}(c_i - \bar{c})^2, \quad i = 1, 2. \tag{4.4}$$

Substitution of (4.4) into (1.2) using (4.1) and (4.3) leads to

$$\bar{\sigma}_0 = \Sigma(\bar{c}) + \frac{1}{2}\frac{\partial^2 \Sigma(\bar{c})}{\partial c^2}\frac{f^{(1)}}{f^{(2)}}(c_1 - \bar{c})^2. \tag{4.5}$$

This result is interesting in several respects. It is independent of $\partial \Sigma(\bar{c})/\partial c$ and depends on $c_1 - \bar{c}$ only quadratically. Since $\partial^2 \Sigma/\partial c^2$ is generally positive (see Fig. 8 for the case of spherical particles), non-uniformity *increases* $\bar{\sigma}_0$ above $\Sigma(\bar{c})$, which is the flow stress for a matrix with uniformly distributed particles and the same average particle volume fraction. The increase occurs if the particle-rich sub-regions are identified with the "particulate" phase ($c_1 > \bar{c}$) or if they are associated with the "matrix" phase ($c_1 < \bar{c}$). Of course, (4.5) is limited to the range of non-uniformity such that (1.2) and (4.4) remain accurate.

A specific example which shows how non-uniformity influences $\bar{\sigma}_0$ for arbitrary $c_1 - \bar{c}$ is shown in Fig. 10. Here, $f^{(1)} = f^{(2)} = \frac{1}{2}$, and $\bar{\sigma}_0$ is determined from $\sigma_0^{(1)}$ and $\sigma_0^{(2)}$ from the stress-averaging curve in Fig. 2. The results apply to rigid spherical particles with $\Sigma(c)$ given in Fig. 8. Curves of $\bar{\sigma}_0/\sigma_Y$ versus $c_1 - \bar{c}$ are plotted for three values of $\bar{c}$. The curves are plotted over the full range of $c_1$ consistent with the constraints that $c_1$ and $c_2$ are non-negative and that neither exceed about 0.62 corresponding to particle touching with $\Sigma$ becoming unbounded.

The curves of Fig. 10 display the quadratic dependence of $c_1 - \bar{c}$ in the vicinity of $c_1 = \bar{c}$ which is implied by (4.5). Now, however, the advantage of distributions with a particle-rich matrix phase becomes evident when $c_1$ is well below $\bar{c}$. This trend is consistent with the fact that the composite must become rigid if the matrix phase becomes rigid but can have a finite flow stress if the particle phase becomes rigid. Perhaps the most significant, non-obvious implication of (4.5), together with the example in Fig. 10, is that, for the class of non-uniform particle distributions modelled here, the uniform distribution is associated with the *lowest* overall flow stress.

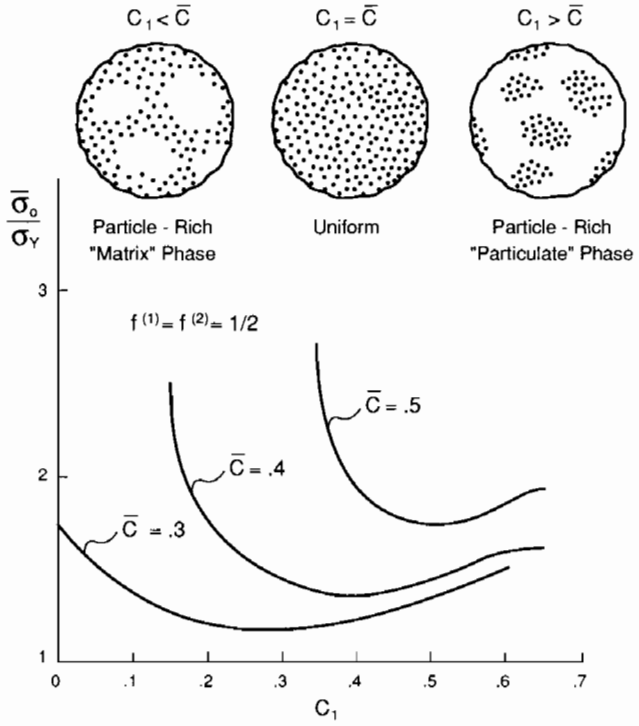


Fig. 10. Dependence of limit flow stress on the degree of non-uniformity of the distribution of equi-sized, spherical reinforcing particles. Predictions for three levels of average particle volume fraction, $\bar{c}$, are shown. Non-uniformity in this plot is proportional to $c_1 - \bar{c}$. The volume fractions of the particle-rich and particle-poor regions are equal, $f^{(1)} = f^{(2)} = \frac{1}{2}$.

**Acknowledgement**

This work was supported in part by the DARPA University Research Initiative (Subagreement P.O. VB38639-0 with the University of California, Santa

Barbara, ONR Prime Contract N00014-86-K0753). The work of JWH was supported additionally by NSF Grant MSM-88-12779 and by Harvard University. Provision of the ABAQUS finite element code by Hibbitt, Karlsson and Sorensen, Inc. of Providence, RI is gratefully acknowledged. The calculations on the FPS 500EA computer were made possible by FPS Computing through the UCSB Industrial Liaison Program.

## References

Bao, G., J.W. Hutchinson and R.M. McMeeking (1991), Particle reinforcement of ductile matrices against plastic flow and creep, *Acta Metall. Mater.*, in press.

Christensen, R.M. (1990), A critical evaluation for a class of micro-mechanics models, *J. Mech. Phys. Solids 38*, 379.

Dendievel, R., G. Bonnet and J.R. Willis (1990), Bounds for creep behavior of polycrystalline materials, *Proc. IUTAM Symp. on Inelastic Deformation of Composite Materials*, to be published.

Hill, R. (1965), Continuum micro-mechanics of elastoplastic polycrystals, *J. Mech. Phys. Solids 13*, 89.

Hutchinson, J.W. (1976), Bounds and self-consistent estimates for creep of polycrystalline materials, *Proc. R. Soc. A 348*, 101.

Hutchinson, J.W. (1977), Creep and plasticity of hexagonal polycrystals as related to single crystal creep, *Met. Trans. A*, 1465.

Taggart, D.G. and J.L. Bassani (1991), Elastic–plastic behavior of particle reinforced composites-influence of residual stresses, *Mech. Mater. 12*, 63.

Weng, G.J. (1990), The overall elastoplastic stress–strain relations of dual-phase metals", *J. Mech. Phys. Solids 38*, 419.